Quantum chemical investigation of a multistate multifunctional molecular switch triggered by two-photon absorption

Deveaux, Noah; Champagne, Benoît; Beaujean, Pierre; Ramos, Tárcius N.; Pires Valverde, Danillo

Published in:
Theoretical Chemistry Accounts

DOI:
10.1007/s00214-025-03214-4

Publication date:
2025

Document Version
Peer reviewed version

Quantum Chemical Investigation of a Multi-State Multi-Functional Molecular Switch Triggered by Two-Photon Absorption

Noah Deveaux[1], Danillo Valverde[2], Pierre Beaujean[1], Benoît Champagne[1], Tárcius N. Ramos[1*]

[1*]Laboratory of Theoretical Chemistry, Namur Institute of Structured Matter, University of Namur, Rue de Bruxelles, Namur, 5000, Belgium.
[2]Laboratory for Computational Modeling of Functional Materials, Namur Institute of Structured Matter, University of Namur, Rue de Bruxelles, Namur, 5000, Belgium.

*Corresponding author(s). E-mail(s): tarcius.nascimento@unamur.be;

Abstract

The two-photon absorption (TPA) cross-section of the dihydroazulene-spiropyran (DHA-SP) multi-state multi-functional dyad has been investigated using quantum chemistry methods to assess its potential as a write nonlinear optical (NLO) switch for 3D data storage. TPA induced switching is found to trigger reactions from DHA-SP to DHA-E-MCH, with TPA cross-sections value of $\sim$ 2500 GM. Conversely to the one-photon absorption, no simple additivity is observed in the dyad TPA spectra but cooperative effects are highlighted in DHA-E-MCH, the most active form. Excitation channel analyses, based on the sum-over-states formalism and the missing state analysis, show that the TPA cross-section of the DHA-E-MCH form mostly result from local excitations on the E-MCH parent unit with important charge transfer contributions from DHA to E-MCH. More generally, it also highlights that the first singlet excited state is the most important excitation channel in all forms presenting large TPA cross-section. This is further confirmed by a simplified three-state model. Overall, the results of this paper demonstrate the promising potential of the DHA-SP multi-state multi-functional molecular switch for NLO read/write applications from the viewpoint of memory devices.

Keywords: Molecular Switches, Two-Photon Absorption, (Time-Dependent) Density Functional Theory, Sum-Over-States (SOS), Linear and Quadratic Responses

Introduction

Modern computing units rely on binary (ON/OFF) solid-state switches of metal-oxide-semiconductor field-effect transistors for processing information. Among the latter, complementary-metal-oxide-semiconductors are the most widely used for the construction of integrated circuits [1]. However, as technologies push the limits of miniaturization, the search for alternatives to traditional silicon-based logic has been intensified in the last years. Enter molecular switches, a class of compounds that can reversibly interconvert between two or more distinct states upon application of external stimuli, leading to changes in their geometrical and electronic structures and, consequently, to modifications of their molecular properties [2]. These dynamic transformations enable molecular switches to perform logic operations [3, 4], making them attractive for a broad range of applications, notably in electronic devices [5, 6] and data storage [7, 8].

To design data storage devices, photochromic molecules serve as key functional units [9] and constitute the substrate (or logic device), with their switching states corresponding to distinct information bits. In such a framework, external stimuli, *i.e.* photons, are referred to as the inputs. This concept extends beyond photochromism to other stimuli-responsive phenomena, such as thermo- and halochromism, where the inputs are heat and changes in pH, respectively [2]. An advantage of photochromic compounds is their ability to undergo isomerizations detectable at the single-molecule level. In principle, if the switching process were perfectly efficient (converting all the molecules, though, experimentally, it often remains partial), each molecule could encode an information bit, enabling high-density storage [10]. An effective strategy

for increasing storage capacity consists in integrating multiple switching units, each addressable by different (orthogonal) stimuli, leading to multi-state multi-functional molecular switches [11–13]. Contrary to bistable switches—only capable of performing simple *YES/NOT* operations—these systems enact multi-valued [14] and multi-input [15] logic functions, allowing for complex gates such as *AND, OR*, exclusive *OR (XOR)*, and exclusive *NOR (XNOR)*, all still at the single-molecule level. In addition, an octa-state switch requires only one-third the number of systems needed for storing the same information as with two-state switches, being a key development for designing high-density storage devices. For example, only eleven molecules are sufficient to represent a larger integer range than a conventional 32-bit architecture.

For molecular switches to be viable for data storage, three key conditions must be met. First, all states must be selectively accessible during writing. This is ensured if the switching is orthogonal [16] or path-dependent [17]. Consider, hypothetically, two bistable units (Fig. 1a) connected by a π-conjugated linker forming a multi-state system where the four possible combinations of states are labeled as [00], [10], [01], and [11]. The resulting switching processes depend on the ability of the multi-state to react under stimuli. In a non-orthogonal switching (Fig. 1b), input 2 switches one unit ([00] $\rightarrow$ [01]), but input 1 leads to [11], which can originate from either [00] or [01], making [10] inaccessible. Conversely, in the case of an orthogonal switching path (Fig. 1c), each input exclusively affects one unit, allowing access to all four states. Furthermore, path-dependent switching (Fig. 1d) ensures unique state accessibility, but [11] is only reachable *via* a specific input sequence (input 2 then input 1). Second, all states must be unambiguously readable. In single-input/single-output devices, linear optical responses (*e.g.*, UV/vis one-photon absorbance, fluorescence, or even electronic circular dichroism) enable fast and cost-effective state discrimination but they lack the ability to focus on small volumes. Finally, the states should be stable for keeping data integrity.

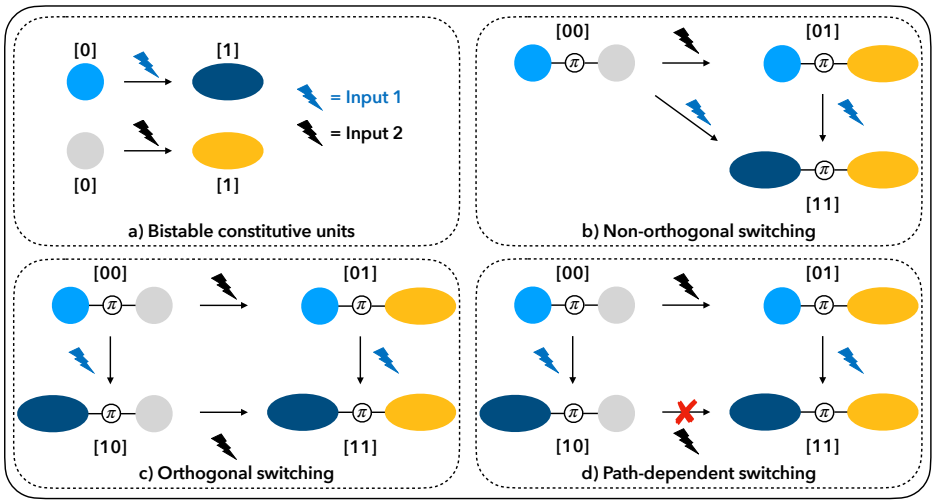

Fig. 1 Stimuli-dependent switching processes in a system composed of two switching units (adapted from Ref. 17).

A complementary approach to increase storage density is the development of three-dimensional (3D) memory architectures [18, 19], enabling storage capacities up to the petabit scale in ultra-compact volumes [20], because the data are written on multiple layers within a stacked wafer assembly rather than on a single surface. Other storage technologies based on photochromic materials have been proposed, such as near-field optical memories, *e.g.*, in the studies of Irie and co-workers using diarylethenes [9, 21]—their promise lies in achieving sub-diffraction-limited storage with fast read/write speeds and ultra-high density. Nevertheless, 3D optical memories are mechanically less challenging and present room for potential improvements in writing speed and storage density. Two-photon writing, relying on two-photon absorption (TPA), is essential for 3D memories. TPA is a nonlinear phenomenon where two photons of low energy are simultaneously absorbed by a molecule, leading to an electronic excitation [22]. It was theoretically predicted by Göppert-Mayer in 1931 [23, 24] but only observed 30 years later by Kaiser and Garret [25] thanks to the apparition of lasers. The GM standard unit of TPA cross-section honors Göppert-Mayer and represents 10^{-50} cm^4 s photon^{-1} while 1 atomic unit = 1.896788 GM. TPA-driven photochemical reactions

can thus occur only at the laser(s) focus, where beams overlap in time and space, which allows to closely pack the functionalized wafers. Beyond high storage capacity and density, TPA writing offers (i) reduced photo-damage, (ii) random access, and (iii) parallel processing [26]. However, writing speeds remain low due to the modest TPA cross-section (σ_{TPA}) of currently used molecular switches. To overcome this, two main strategies exist for designing new compounds with high σ_{TPA} values, that also possess low absorption wavelengths to further reduce the bit spacing in 3D storage devices. One approach aims to design molecular switches presenting high TPA cross-sections [26, 27] for direct applications, while, alternatively, the TPA-active molecule can act as an "antenna" to transfer energy to a switchable unit [28].

Complementary, the ability of reading high-density information is crucial for the development of 3D optical memories and TPA can also be used for reading purposes, although it may partially degrade stored data by inducing undesired switching. In this context, the second harmonic generation (SHG), a second-order nonlinear optical (NLO) property governed at the molecular scale by the first hyperpolarizability (β) [29], becomes an interesting alternative to avoid data degradation under reading. Hence, SHG-readable switches must exhibit strong β-contrasts between their states [30–32].

Recently, Dowds *et al.* [17] proposed and characterized a multi-state multi-functional switch integrating the 2-phenyl-1,1-dicyano-1,8a-dihydroazulene (DHA) bistable unit with the multi-state 1',3',3'-trimethyl-6-nitroindolinobenzospiropyran (SP) moiety. Fig. 2 illustrates the switching behavior of this DHA-SP dyad, which exhibits both orthogonal and path-dependent transitions, generating a total of eight distinct states in solution (excluding stereoisomers) by combining light irradiations and pH variations. Photoexcitation at 415 nm promotes the stable DHA isomer to its lowest singlet excited state, triggering a ring-opening towards the higher-energy vinylheptafulvene (VHF) isomer [33–35]. On the other side of the linker, a 365 nm

irradiation induces C–O bond cleavage, triggering SP ring-opening in VHF-SP to form a zwitterionic merocyanine (VHF-MC) [36]. Additionally, in DHA-SP, both units can switch non-orthogonally to VHF-MC under 365 nm light illumination. Adding acid to the photo-metastable MC yields a protonated *transoid* merocyanine (E-MCH). These states were characterized by their one-photon absorption (OPA) and fluorescence properties, acting as readouts. Moreover, the reverse VHF-MC → VHF-SP → DHA-SP reactions are spontaneous and thermally driven. The VHF-SP, VHF-MC, and VHF-E-MCH *trio* of states acts as an *AND* logic gate: transitioning to the fluorescent VHF-E-MCH form requires both 365 nm irradiation *AND* acid addition—if either condition is unmet, no emission occurs. Finally, acidification of SP (in both DHA and VHF forms) directly produces the protonated *cisoid* merocyanine (Z-MCH). In the Dowds *et al.* [17] study, one drawback is the use of monochromatic light as input and OPA as the output, which increases the probability of switching during the reading process. To overcome this undesired effect, some of us examined the DHA-SP potential as an NLO switch for non-destructive reading *via* SHG using computational quantum chemistry methods [37]. It was shown that combining the hyper-Rayleigh scattering intensities and their depolarization ratios enables multi-state distinction.

For memory applications, molecular switches are typically grafted onto surfaces or embedded in polymers matrices making acidochromism impractical [38, 39]. However, this multi-switch serves as an excellent model. Indeed, SP-MC derivatives have been extensively studied [36, 40] and were used in the first demonstration of a 3D optical memory [41], while DHA has also been explored for multi-dimensional data storage [42]. However, to the best of our knowledge, all attempts of TPA induced switching for 3D storage have relied exclusively on two-state switches, and the TPA induced switching of DHA-SP multi-state has not yet been investigated.

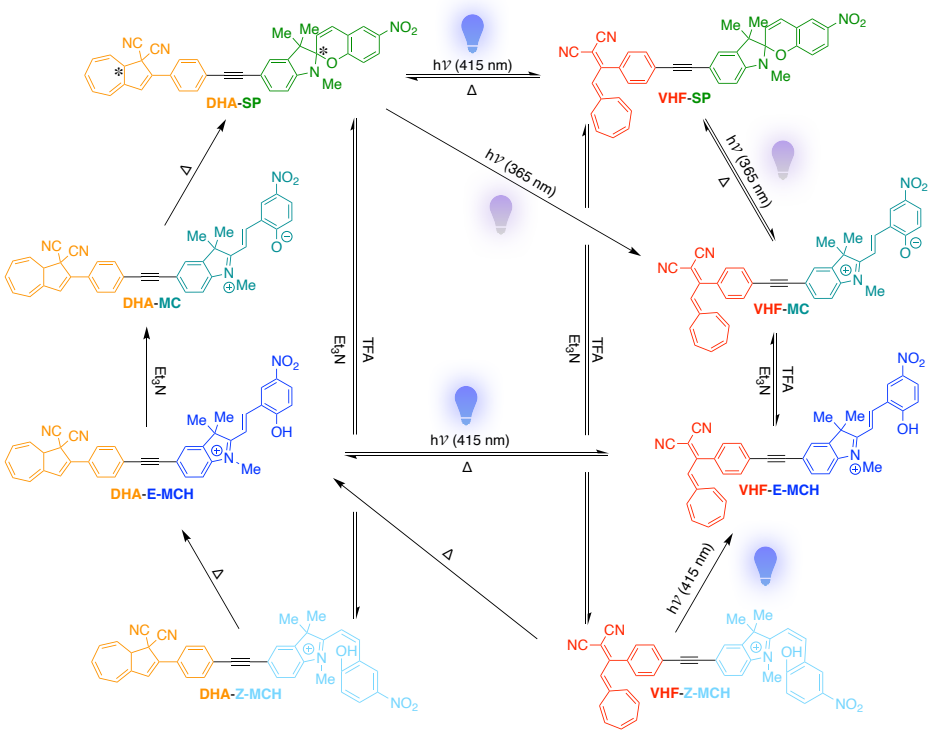

Fig. 2 Overview of the switching reactions of the DHA-SP dyad (adapted from Ref. 17), TFA: trifluoroacetic acid, '∗' refers to the asymmetric centers of the DHA-SP form, and the bulbs highlight the photo-triggered reactions.

This Account presents a computational quantum chemical investigation of the TPA properties of the DHA-SP dyad in solution, employing (time-dependent) density functional theory [(TD)-DFT] to analyze its full potential as a read/write NLO switch before advancing to more complex 2D and 3D architectures, usually more challenging to establish. Building upon the experimental characterizations [17] and our previous theoretical endeavors [37], TPA is introduced as a novel writing mechanism for this molecular multi-state switch. The focus is on the forms capable of undergoing a light-triggered switching transition, *viz.* DHA-SP, DHA-E-MCH, VHF-SP, VHF-Z-MCH, and their parent units (which also include the linker with an hydrogen substituting the second unit). The photo-reactions originating from the latter are highlighted with

bulbs in Fig. 2. The work is structured as follows. The next Section presents the essential of the theoretical and computational aspects. Results are then exposed, beginning with the one- and two-photon absorption spectra and an analysis of the charge transfer character, complementing the discussion in Ref. 37. This is followed by a comparison of the two computational formalisms used to determine the TPA responses. These responses are then further rationalized by considering the contribution of individual electronic excited states. Finally, conclusions are drawn and several perspectives are proposed.

Theory and calculation aspects

Quantum chemistry calculations

The ground state optimized geometries of all the states related to the molecular switching processes of the dyad, as presented in Ref. 37, were obtained by minimizing their energy using the ωB97X-D [43] exchange-correlation functional (XCF) with the 6-311G(d) basis set. The OPA and TPA transition energies and intensities (oscillator strengths/TPA transition probabilities, respectively) were obtained using TD-DFT within the linear (LR) and quadratic response (QR) formalism, respectively. Benchmarks assessing the performance of different XCFs on molecules presenting a charge-transfer (CT) excitation character have recommended the use of range-separated XCFs, even though the obtained excited-state dipole moments tend to be underestimated [44, 45]. In this study, the optical responses were obtained with the CAM-B3LYP [46] XCF combined with the 6-311+G(d) basis set, employing the Dalton2020.1 program [47]. The acetonitrile solvent effects were taken into account using the FixSol, a continuum conductor-like model assuming the value of 36.640 for the relative static dielectric constant and 1.806 for the optical one [48], as implemented in the Polarizable Embedding library [49].

The transition dipole moments between the ground ($|g\rangle$) and excited ($|n\rangle$) states ($\langle g|\boldsymbol{\mu}|n\rangle$) as well as the excitation energies associated with the transitions [$\hbar\omega_{gn} = \hbar(\omega_n - \omega_g)$] are the main ingredients for simulating the OPA spectrum. The OPA cross-section [$\sigma_{\mathrm{OPA}}(\omega)$, Eq. 1] is given by

$$\sigma_{\mathrm{OPA}}(\omega) = \frac{4\pi^2}{3\hbar c}\omega \sum_{n\neq g} \left\{ [M_{gn}^{(1)}]_x^2 + [M_{gn}^{(1)}]_y^2 + [M_{gn}^{(1)}]_z^2 \right\} \mathcal{G}(\omega, \omega_{gn}; \Gamma) \tag{1}$$

$$[M_{gn}^{(1)}]_i = \langle g|\mu_i|n\rangle, i = x, y, z \tag{2}$$

$$\mathcal{G}(\omega, \omega_{gn}; \Gamma) = \frac{1}{\Gamma}\sqrt{\frac{\ln 2}{\pi}} \exp\left(-\frac{\ln 2(\omega - \omega_{gn})^2}{\Gamma^2} \right) \tag{3}$$

where $\hbar\omega$ is the photon energy, c is the speed of light in vacuum, $\boldsymbol{M}_{gn}^{(1)}$ is the one-photon transition moment vector coupling the ground and excited states. The function $\mathcal{G}(\omega, \omega_{gn}; \Gamma)$ is a Gaussian broadening function that accounts for the dynamical fluctuations of the dyad in solution and depends on the broadening factor Γ, which represents the half-width at half-maximum (HWHM). The oscillator strength is given by $f_{gn} = 2\hbar\omega_{gn}|\boldsymbol{M}_{gn}^{(1)}|^2/3$.

The TPA transition probability ($\delta_{gn}^{\mathrm{TPA}}$, Eq. 4) depends on the light polarization factors F, G, H and on the TPA transition moment tensor ($\boldsymbol{M}_{gn}^{(2)}$, Eq. 5) induced by a pair of photons with energies $\hbar\omega_1$ and $\hbar\omega_2$ [50].

$$\delta_{gn}^{\mathrm{TPA}} = \frac{1}{30} \sum_{i,j=x,y,z} F[M_{gn}^{(2)}]_{ii}[M_{gn}^{(2)}]_{jj} + G[M_{gn}^{(2)}]_{ij}[M_{gn}^{(2)}]_{ij} + H[M_{gn}^{(2)}]_{ij}[M_{gn}^{(2)}]_{ji} \tag{4}$$

$$[M_{gn}^{(2)}]_{ij} = \frac{1}{\hbar} \sum_k \frac{\langle g|\mu_i|k\rangle\langle k|\mu_j|n\rangle}{\omega_{gk} - \omega_1} + \frac{\langle g|\mu_j|k\rangle\langle k|\mu_i|n\rangle}{\omega_{gk} - \omega_2} \tag{5}$$

Equation 5 is referred to as the sum-over-states (SOS) expression for the TPA transition moments because it sums over the $|k\rangle$ states. Note that in Eq. 5, the ground and final states are included in the sum and all the other states are commonly referred to

as intermediate states. This expression is usually related to the imaginary contribution of the resonant second hyperpolarizability [$\Im\{\gamma(-\omega;\omega,-\omega,\omega)\}$] associated with the degenerate four wave mixing phenomenon [51, 52].

This study assumes degenerate photons ($\omega_1 = \omega_2 = \omega$) and parallel polarization of a linearly polarized light beam ($F = G = H = 2$). The TPA cross-section [$\sigma_{\mathrm{TPA}}(\omega)$, Eq. 6] is then formulated to match experimental results obtained using a single light source [44, 50, 53], *e.g.*, the Z-scan technique [54].

$$\sigma_{\mathrm{TPA}}(\omega) = \frac{4\pi^3}{c^2}\omega^2 \sum_{n\neq g} \delta_{gn}^{\mathrm{TPA}} \mathcal{G}(2\omega, \omega_{gn}; \Gamma) \tag{6}$$

It is important to note that the energies will be hereafter discussed in terms of the transition energies ($\hbar\omega_{gn}$) for a better association with the OPA spectra and not in terms of the photon energy ($\hbar\omega = \hbar\omega_{gn}/2$).

Computing Eq. 5 using the SOS approach requires computing the excitation energies ($\hbar\omega_{gk}$), dipole moments of the ground ($\langle g|\boldsymbol{\mu}|g\rangle$) and excited ($\langle k|\boldsymbol{\mu}|k\rangle$) states, and ground-to-excited ($\langle g|\boldsymbol{\mu}|k\rangle$) as well as excited-to-excited ($\langle k|\boldsymbol{\mu}|k'\rangle$) state transition moments. Moreover, achieving convergence for the SOS quantity may require a large number of intermediate states, increasing the computational cost. Consequently, most studies have used semi-empirical Hamiltonian approximations [52, 55–59]. However, simplifying the SOS expression to include only dominant-state contributions has led to the successful application of truncated few-states models using higher-level calculations for TPA transitions exhibiting CT character [60–63].

Alternatively, the full SOS quantity $[M_{gn}^{(2)}]_{ij}$ (Eq. 5) can be efficiently extracted from the QR function vector [64–66]. Methods with different levels of accuracy have been developed based on this approximation (ranging from wavefunction-based methods, such as coupled cluster and multiconfigurational approaches, to TD-DFT and its

simplified variations), allowing researchers to find a reliable cost-accuracy balance for small to large molecules [44, 59, 67–73].

The QR formalism offers an efficient computational approach to directly extract TPA transition moments from the second-order perturbed response vector [64], although it has been showed that the presence of the XCF in the DFT formalism can lead to incorrect description of the QR function poles, essential for obtaining the TPA transition moments [74]. Moreover, in such QR scheme that provides the global response, a detailed description of the excitation channels is lacking, as these quantities cannot be decomposed into contributions from the intermediate states involved in the sum.

Excitation channels analysis

To analyze the excitation channels, Eq. 5 must be calculated using the ordinary SOS formalism to decompose the TPA transition moments into the contributions of different excited states. This was then performed by using the ground and excited states dipole moments, transition dipole moments between each pair of the ground-to-excited and excited-to-excited states, and vertical excitation energies from the 100 lowest-lying excited states, obtained from the relaxed one-particle density at the linear response level. To this aim, one-electron transition density matrix (1TDM) was reconstructed using the configuration state functions coefficients larger than 10^{-8} from TD-DFT calculations, and then the (transition) dipole moments were calculated using the Multiwfn program [75, 76]. As a consequence, while ground-to-excited state quantities are true TD-DFT values, the excited-to-excited ones as well as excited state dipole moments are approximations. Indeed, they correspond to the "unrelaxed approximation" of Ref. 74 as they lack the so-called orbital relaxation [77]. They are thus not equivalent to the values obtained through QR, but, as mentioned earlier, this approach can still provide interesting insights by addressing the excitation channels involved in the transitions.

Finally, the TPA transition moments were calculated using a homemade software, where the excitation channels were analyzed in terms of the contributions of the different intermediate states. To do so, the contributions to the TPA cross-sections of specific intermediate states included in the SOS formula were evaluated by employing the missing state analysis [78]. It involves doing a series of truncated SOS calculations, in which one state of the sum (running here over the 100 first excited states) is left out. The contribution of the i^{th} intermediate excited state in the $S_0 \rightarrow S_n$ transition (ϑ_i^n) is determined by the effect of its absence on σ_{TPA} of the final state:

$$\vartheta_i^n = \frac{\sigma_{\mathrm{TPA}}^{tot} - \sigma_{\mathrm{TPA}}^{i}}{\sigma_{\mathrm{TPA}}^{tot}}, i \neq n \tag{7}$$

where $\sigma_{\mathrm{TPA}}^{tot}$ is the SOS value with no state missing (here encompassing 100 excited states), and $\sigma_{\mathrm{TPA}}^{i}$ is the one where state i is missing. A missing state coefficient of zero implies that the intermediate state does not contribute to the response, while a negative ϑ_i^n indicates that state i interacts destructively, thereby reducing σ_{TPA}. Yet, ϑ_i^n is limited to +1 because σ_{TPA} is positively defined, meaning the i state fully dominates the excitation. For simplicity, ϑ_i^n is referred to as ϑ_i throughout this article, except when specific final states must be explicitly distinguished.

Charge transfer characterization

The character of the singlet excited states of the molecular dyads was analyzed using the TheoDORE package (version 3.2) that allows to easily assign the electronic nature of a given excited state from a fragment-based analysis using the 1TDM [79]. Mathematically speaking, the main idea is the transformation of the 1TDM from the molecular orbital (MO) basis representation ($\mathbf{T}$) to the atomic orbital (AO) basis ($\tilde{\mathbf{T}}$) followed by a Löwdin orthogonalization scheme given that the AOs are usually non-orthogonal. In this context, the charger transfer number (Ω_{AB}) is interpreted as the

one-electron character of the excitation, or in other words, it measures the total contribution of excitations (forward or backward) from any atom of fragment A to B or *vice versa*. This quantity is expressed as follows:

$$\Omega_{\mathrm{AB}} = \sum_{\mu \in \mathrm{A}} \sum_{\nu \in \mathrm{B}} \left[\left(\mathbf{S}^{1/2} \tilde{\mathbf{T}} \mathbf{S}^{1/2} \right)_{\mu,\nu} \right]^2 \tag{8}$$

where $\mathbf{S}$ is the AO overlap matrix and the double sum runs over all atoms in fragments A and B, respectively.

In order to carry out these analyses, two fragments are adopted for the molecular dyads with the C≡C bond defining the frontier region. In addition, the TheoDORE program was fed by the Dalton output results parsed by the cclib library version 1.8 [80].

Results

This section aims at rationalizing which compounds are more prone to be excited *via* a two-photon absorption process. It is firstly worth mentioning that the OPA spectra of these molecules were extensively discussed in our previous work and cross-compared with the available experimental results [37].

One-photon absorption spectra

Starting with the discussion of the OPA spectra (based on the 10 lowest energy excited states, Fig. 3, blue lines), the DHA-SP compound shows a broad and intense absorption band with a peak centering at 3.18 eV and a shoulder around 4 eV. This absorption band is essentially composed by the two lowest-lying singlet excited states. The $S_0 \rightarrow S_1$ transition is mostly characterized by local excitations (LE) on the DHA unit ($\sim$ 80%), as shown in Fig. 4a, whereas for the $S_0 \rightarrow S_2$ transition, there are significant contributions coming from LE inside the SP fragment ($\sim$ 20%) and charge transfer

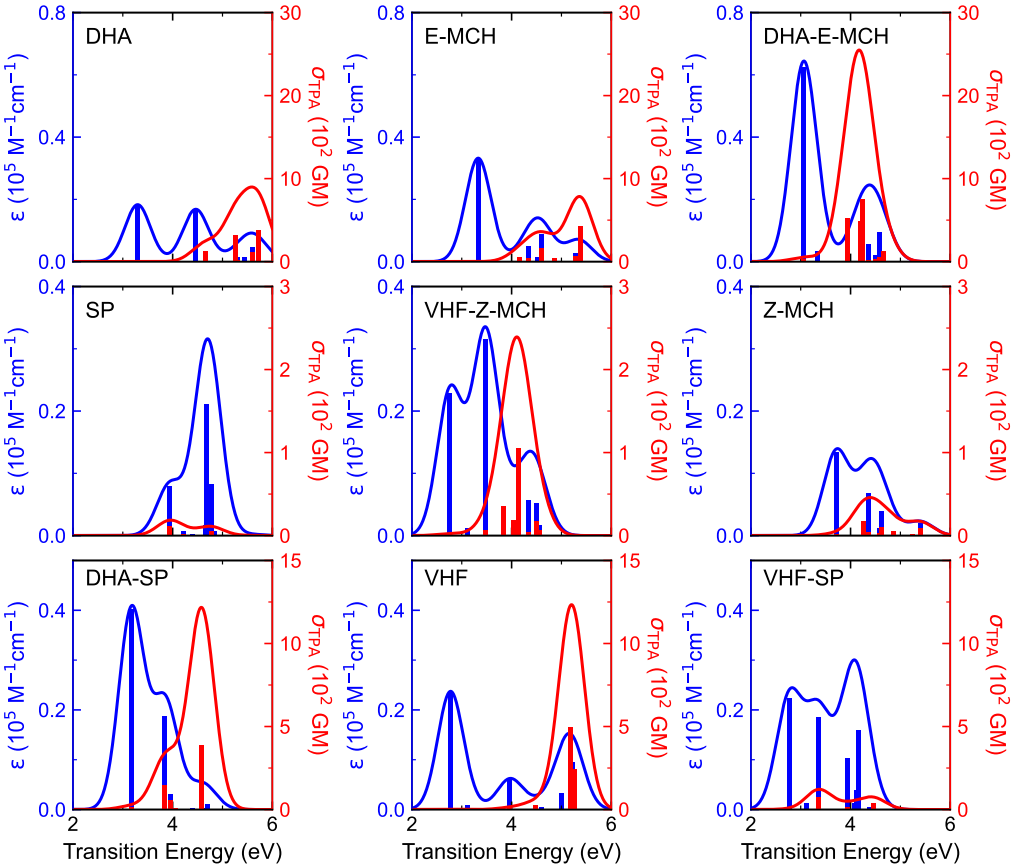

Fig. 3 OPA (blue line) and TPA (red line) spectra of the molecular dyads and their respective parent units computed at the TD-CAM-B3LYP/6-311+G(d) level ($\Gamma = 0.3$ eV). All TPA spectra are convoluted using the σ_{TPA} values calculated from the quadratic response formalism.

(CT) from SP to DHA ($\sim$ 20%), in addition to the LE on the DHA moiety ($\sim$ 50%). In comparison with the DHA parent unit, the absorption peak is red-shifted from 3.18 eV (DHA-SP) to 3.30 eV (DHA), which agrees with the measured experimental red-shift of 0.1 eV [17]. The SP unit does not contribute to this energy range of the DHA-SP OPA spectrum because its excited states lie above 4 eV.

The first peak associated with the DHA-E-MCH OPA spectrum is in the same energy region as that of DHA-SP, but having a stronger intensity. This higher intensity is explained by the electronic nature of the $S_0 \rightarrow S_1$ transition, since it has a

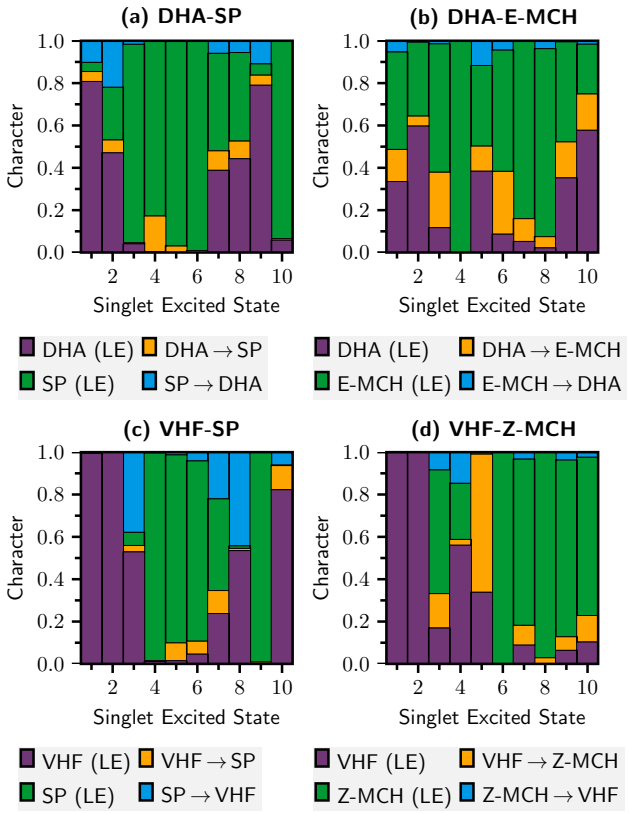

Fig. 4 Fragment-based analysis of the 10 lowest-lying singlet excited states for (a) DHA-SP, (b) DHA-E-MCH, (c) VHF-SP, and (d) VHF-Z-MCH computed at the TD-CAM-B3LYP/6-311+G(d) level.

considerable contribution of excitations coming from the E-MCH unit ($\sim$ 40%) over the DHA ($\sim$ 30%) (Fig. 4b), indicating a strong additivity of the parent units spectra. This contrasts with the dominant LE contribution from DHA on the DHA-SP compound. Moreover, there is a second absorption band originated from the S_{3-6} excited states around 4.3 eV.

The VHF-SP spectrum shows a broad absorption band including several intense transitions (S_1, S_3, S_4, and S_7). From the fragment-based analysis, the two lowest-energy excitations are fully dominated by LE on the VHF unit Fig. 4c, such that these two transitions have identical excitation energies compared to its VHF parent (see Table S1 and S2). Besides, the $S_0 \rightarrow S_3$ transition presents an important

CT contribution from SP to VHF units ($\sim$ 40%). The VHF-Z-MCH form presents a similar electronic structure to VHF-SP, and, as a consequence, the electronic transitions driving to the S_1 and S_2 states have the same excitation energies and oscillator strengths as the VHF parent unit. However, it presents an intense absorption band centered around 3.5 eV, corresponding to the third excited state, which has a large LE contribution on the Z-MCH moiety ($\sim$ 60%).

Two-photon absorption spectra from quadratic response function

Turning now to the TPA spectra (based on the 10 lowest energy excited states, Figure 3, red lines), the DHA and E-MCH parent units exhibit similar TPA profiles, with an intense σ_{TPA} band centered around 5.5 eV ($\sim 10 \times 10^2$ GM) and a shoulder around 4.5 eV. The VHF compound also presents an intense σ_{TPA} ($\sim 12 \times 10^2$ GM) around 5.5 eV. Conversely, low σ_{TPA} (0.2×10^2 GM at 4.0 eV) intensities are obtained for the SP molecule. Similarly, the σ_{TPA} maximum value for the Z-MCH form reaches 0.3×10^2 GM at 4.3 eV.

For the molecular dyads, the DHA-SP TPA spectrum has an energy band centered at 4.6 eV with an impressive TPA cross-section ($\sim 12 \times 10^2$ GM). This absorption band is mainly composed by two degenerated high-energy excited states (S_7 and S_8). Both transitions bear a similar electronic nature, being fundamentally characterized by LE on DHA and SP units (Fig. 4a). In addition, the $S_0 \rightarrow S_2$ transition is responsible for the shoulder that appears at 3.9 eV and is mainly characterized by LE in the DHA unit. Replacing DHA with VHF leads to a slight red-shift in the spectrum and a strong decrease of intensity to less than 1.5×10^2 GM. Moreover, its σ_{TPA} spectrum resembles its parent SP unit, leading us to conclude that the contribution coming from its parent VHF unit would appear at much higher energies (above 5 eV). Note that, in this energy region, the photon energy ($\hbar\omega = 2.5$ eV) starts to induce the OPA

phenomenon ($\hbar\omega_{g1} = 2.77$ eV). Next, replacing the SP unit with Z-MCH, which gives rise to the VHF-Z-MCH molecule, slightly enhanced the σ_{TPA} (2.4×10^2 GM) and blue-shifted the peak to 4.1 eV. According to the CT analyses, the excitation that provides the highest σ_{TPA} value is mostly localized on the Z-MCH moiety, showing again that the parent VHF unit does not contribute on the σ_{TPA} spectrum. This finding also evidences how a moiety replacement can substantially affect or not the σ_{TPA} intensity. In fact, the effects on the TPA are stronger than on the OPA.

Among the studied molecules, the DHA-E-MCH is the one that shows the highest σ_{TPA} ($\sim 25 \times 10^2$ GM) and therefore it would be the best candidate to TPA molecular switch applications. This intense band results from transitions to three excited states (S_3, S_5 and S_6) with all of them being described by single excitations delocalized over the DHA and E-MCH units. According to the fragment-based analysis, the S_3 and S_6 state has a predominant LE contribution in the E-MCH unit ($\sim 65\%$ for both states), while S_5 is a mix of LE contributions on both units (around 40% in each fragment).

Two-photon absorption from the SOS scheme

Alternatively to the QR formalism for computing the σ_{TPA}, the SOS approach can be used at a reasonable computational cost using the 1TDM to reconstruct the excited state wavefunctions. It directly connects to the CT analyses (also based on the 1TDM) and allows a further description of the TPA excitation channels. Before breaking down the SOS into the missing state analyses, a direct comparison between the σ_{TPA} obtained using QR and SOS is presented.

Fig. 5 shows that the shape of the spectra are mostly preserved between the two approaches, except for VHF, but with only slightly larger intensities when SOS is used. On the one hand, for DHA-SP, DHA-E-MCH, and VHF-Z-MCH, both methods yield nearly identical TPA spectra. On the other hand, the SOS approach leads to σ_{TPA} values up to 4 times larger compared to QR for VHF, the form which presents

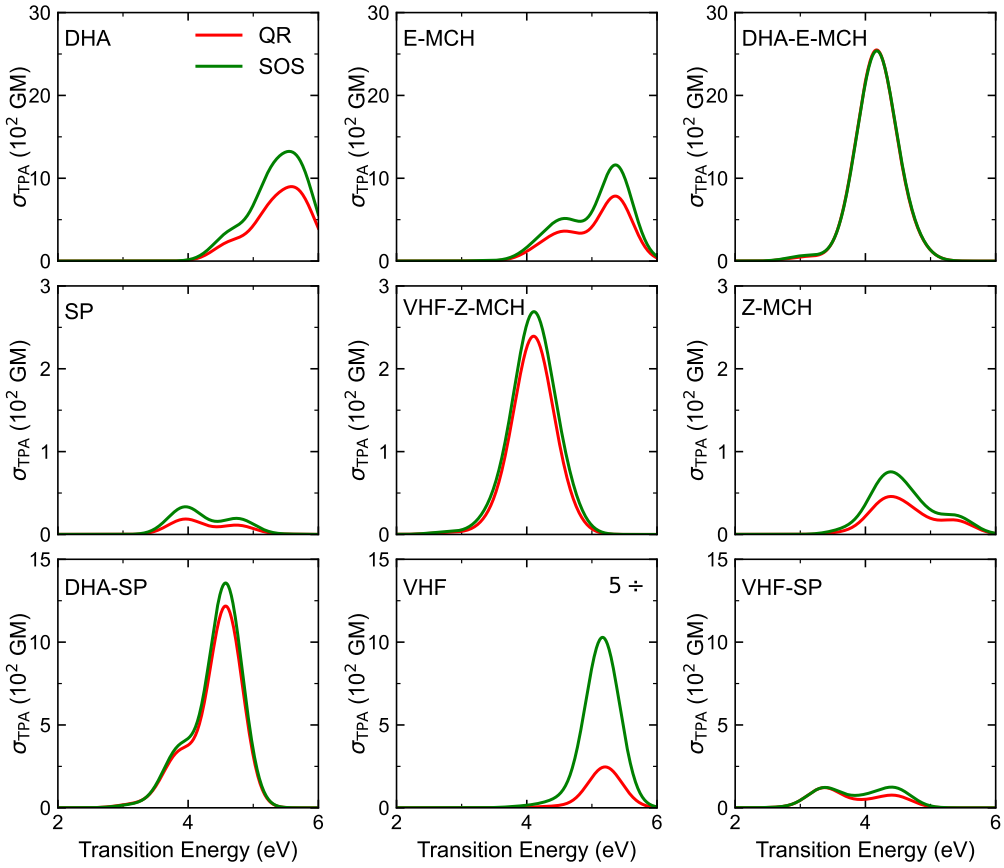

Fig. 5 Comparison between the TPA spectrum computed using the quadratic response (red line) and sum-over-states (dark red line) approaches of the molecules dyads and their respective parent units. A scale factor of 1/5 is used in the spectrum of VHF to improve readability.

the lowest σ_{TPA} value. It was not possible to find a correlation between this behavior and other quantities, such as the CT character of the different states implicated in the transition. This difference could therefore be attributed to different factors: the absence of orbital relaxation in the contributions to the SOS expression, the need for further excited states to converge the sum, or inaccuracies in the TD-DFT approach for computing the QR poles, and, therefore, the TPA transition moments [74]. To explain the spectra, the next section explores the missing state analysis, which disentangles the contributions of individual states to the total TPA response.

Interpretation of the σ_{TPA} *via* the missing state analysis

A deeper understanding of the TPA cross-sections was grasped through the missing state analysis, based on a series of SOS calculations (Eq. 7). Fig. 6 shows a heat map of the relative contributions (ϑ_i) from the 35 lowest-energy intermediate excited states included in the SOS expression to σ_{TPA} of the 10 lowest-energy TPA-accessible (final) states of DHA-E-MCH. Cells in black indicate that the ϑ_i^i coefficients were removed from the analysis because it is the target final state. The corresponding plots for the remaining dyads and parent units are presented in Figures S2 and S3.

In general, when a final state has a large TPA cross-section (such as S_7 and S_8 in DHA-SP, or S_5 and S_6 in DHA-E-MCH), only a few excited states significantly contribute, typically with the dominant excitation channel going through S_1 ($\vartheta_1 \sim 1$), regardless of the CT nature of the one-photon excitation. Indeed, for the TPA active forms of the dyads and their parent units, the oscillator strengths associated with the $S_0 \rightarrow S_1$ transitions are relatively large (ranging from 0.7 to 2.5). Consequently, a three-state approximation should suffice to reproduce the main TPA spectral bands for these forms (*vide infra*). In contrast, when σ_{TPA} is near zero—for instance, for most TPA states of SP or for S_1, S_4, S_7, and S_8 in DHA—a larger number of intermediate states contributes, often with negative ϑ_i values.

Turning specifically to DHA-E-MCH, which exhibits the highest TPA activity among the studied dyads and the best agreement between the SOS and QR approaches, it is observed that S_1 also strongly influences the TPA cross-section of all the dominant TPA-active states (*viz.* S_3, S_5, and S_6). Since the one-photon transition to S_1 has been identified as involving both switching units, primarily as a simultaneous local excitation on each unit, and since both units are individually TPA-active, the intense TPA response of DHA-E-MCH is attributed to their cooperative contribution. The excited states adjacent in energy to S_5 and S_6 are observed to exert minimal influence on their TPA cross-sections, confirming that the TPA is governed by a transition from

the ground state to the final state with a single channel through S_1. Then, for S_3, the TPA path also involves a significant destructive channel related to the sixth excited state ($\vartheta_6^3 = -0.4$), despite its higher excitation energy ($\hbar\omega_{gn} = 4.23$ eV) and weak oscillator strength for the $S_0 \rightarrow S_6$ transition ($f_{gn} = 0.16$). It indicates that S_6 is strongly coupled to other excited states.

On the contrary, the TPA activity of the S_7 and S_8 states in DHA-SP is primarily attributed to the DHA moiety. This is supported by the CT analysis, which indicates that the $S_0 \rightarrow S_1$ transition is localized on DHA. Then, while the VHF's TPA spectrum exhibits similar intensity to the DHA, its activity is completely suppressed in that energy region when connected to SP and Z-MCH. This is accompanied by the loss of a well-defined two-photon excitation pathway through S_1 in these dyads, whereas it remains intact for the VHF parent. Nonetheless, the missing-state analysis confirms that the overestimation of VHF's σ_{TPA} using the SOS method, compared to the QR approach, arises from approximations in both methods. Indeed, the domination of a few excitation channels including low energy excited states discards the hypothesis of requiring even more (high energy) excited states. This is the case in VHF's TPA, unambiguously dominated by a single channel through S_1.

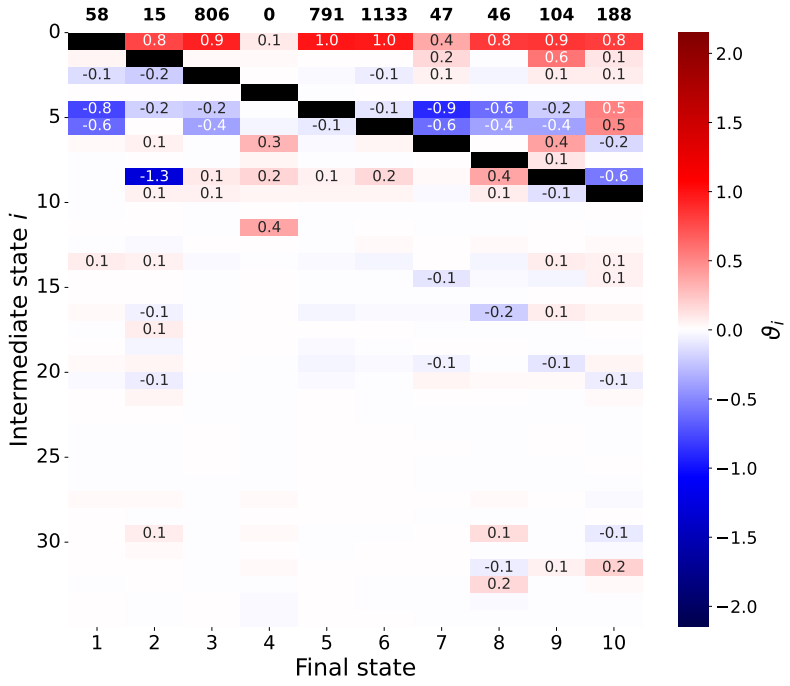

Fig. 6 Relative importance of state i, ϑ_i (dimensionless), to σ_{TPA} of the DHA-E-MCH dyad, as evaluated using the missing state analysis (Eq. 7). ϑ_i with absolute values exceeding 0.1 are labeled on the maps. The σ_{TPA} (GM) values, computed by including the 100 lowest excited states in the SOS formula (using a Gaussian broadening with $\Gamma = 0.3$ eV), are displayed atop the figures for each TPA-accessed state. Cases where the final TPA state corresponds to the missing state are represented in black.

Subsequently, a series of three-states model calculations were performed for DHA-E-MCH and VHF-Z-MCH, considering only the ground state, the final TPA state, and S_1 as the intermediate state. These calculations were carried out for the 10 lowest TPA states, and the results are presented in Table 1, alongside the cross-sections obtained using the full set of 100 intermediate states for comparison. As expected, the two approaches yield consistent results when σ_{TPA} is large, as it is primarily driven by the S_1 pathway, particularly for the S_5 and S_6 final states in DHA-E-MCH. However, for S_3, the absence of S_6 as an intermediate state leads to a 50 % overestimation of σ_{TPA}.

In VHF-Z-MCH, the lack of a clear excitation channel results in a poor description of TPA properties within the three-state approximation, even failing to reproduce the trends in the final state responses, except when the responses are (very close to) zero.

Table 1 Three-states model analyses of the σ_{TPA} for DHA-E-MCH and VHF-Z-MCH dyads. The calculations include contributions from the ground state, the first singlet excited state, and the final TPA state within the SOS expression (using a Gaussian broadening with $\Gamma = 0.3$ eV). Results obtained using the full 100-state model along with their corresponding ratios (3 states / 100 states) are also presented.

Final state	1[1]	2	3	4	5	6	7	8	9	10
DHA-E-MCH										
3 states	144	35	1220	0	927	1086	85	66	96	50
100 states	58	15	806	0	791	1133	47	46	104	188
Ratio	2.48	2.33	1.51	-	1.17	0.96	1.81	1.43	0.92	0.27
VHF-Z-MCH										
3 states	3	0	31	19	32	0	4	9	4	19
100 states	3	0	18	63	43	0	168	17	25	28
Ratio	1.00	-	1.72	0.30	0.74	-	0.02	0.53	0.16	0.68

[1]In this case, a two-state model was employed including only the ground state and the first excited state as final state in the SOS expression.

Conclusions

The two-photon absorption properties of the dihydroazulene-spiropyran multi-state multi-functional dyad proposed by Dowds *et al.* [17] have been computed in solution (implicit solvation) using the quadratic response and sum-over-state methods. Our previous theoretical study [37] has shown that the photo-switching reactions can be be monitored by SHG combining the Hyper-Rayleigh scattering responses and their depolarization ratios. Evaluating the TPA cross-sections of these dyads assesses its full potential as a read/write NLO switch. The focus of the present Account has hence been on evaluating the high-resolution writing aspects induced by TPA photo-switching.

Two TPA-switching reactions have been identified from DHA-SP and DHA-E-MCH. For the former, the most intense TPA has been found to occur in the high-energy S_7 and S_8 states ($\hbar\omega_{gn} \sim 4.2$ eV), making the VHF-MC form the most probable

product. In contrast, TPA of DHA-E-MCH leads unambiguously to the VHF-E-MCH state, as it already occurs with a low lying excited state (S_3, around 810 GM), as well as in the S_5 and S_6 states, with cross-sections exceeding 790 and 1000 GM, respectively. Conversely to the close additivity observed on the OPA spectra, the maximum of the TPA cross-section spectrum observed for DHA-E-MCH is around 60 % larger than the merely additive parent units spectra. The intense transitions present mixed local (within each parent unit) and charge transfer (between the units) contributions, indicating a strong coupling and cooperative effects between the DHA and E-MCH units. These effects are attributed to structural similarities between the parent units—π-conjugated coplanar segments with donor and acceptor groups at the extremities—responsible for large transition dipole moments and large variations of dipole moments upon excitation.

Generally, a good agreement between the TPA cross-sections obtained using the QR and SOS approaches is observed, allowing for understanding the excitation channels involved in the intense transitions. Both missing state and simplified three-states model analyses show that the main TPA channel involves the S_1 intermediate state whenever the cross-section is significant. However, the charge transfer character associated with the excitations to the intermediate or final state are not directly connected with the TPA amplitudes. It has been further emphasized that the high TPA amplitude of DHA-E-MCH results from cooperative contributions of both switching units, whereas the slightly lower amplitude observed for DHA-SP originates solely from the DHA moiety.

Moreover, excited-state dynamics starting in high-energy states may lead to diverse decay pathways, potentially impacting the switching process. Despite this, the use of short-wavelength lasers remains advantageous for achieving narrow bit spacing in 3D optical memories. From the methodological point of view, it is also worth recalling that all calculations were performed on the global minimum of the ground state potential

energy surfaces due to small conformational effects observed on spectroscopic properties of these systems [37]. Therefore, the effects of conformational diversity were not addressed except by the large broadening function parameter. Dynamic conformational effects are known to impact the excited state energy and its ordering as well as the (OPA and TPA) transition dipole moments. However, a quantitative deviation depends on the flexibility of the compounds and also on the solute-solvent interactions [59, 81–85]. Therefore, further studies can help to assess a more complete characterization of the DHA-E-MCH dyad. In addition, the SOS approach allows for easily predicting the TPA cross-section for non-degenerate photons, opening new excitation dynamics investigations. Then, in order to better understand the response of the different systems and complementary to the decomposition into excitation channels provided by the SOS approach, other fragment-based decomposition schemes can be applied [86, 87].

Finally, the results have highlighted the potential of the DHA-E-MCH dyad as a TPA photo-switch, also suggesting molecular designers to be inspired by this chromophore to focus on the strong coupling between the DHA and the E-MCH moieties, and SP at a lesser extent. The DHA-SP multi-state molecular switch therefore demonstrates promising potential for NLO read/write applications from the viewpoint of a 3D memory device, allowing for triggering at least two switching reactions.

Supplementary information. The supplementary information contains: (i) a PDF document, containing the data that supports the findings of this study, (ii) an archive containing the Cartesian coordinates of the computed geometries, as XYZ files, and (iii) an archive containing the SOS file with all, ground state, excited state, and transition dipoles moments, as obtained from Multiwfn and used as input for our homemade code.

Acknowledgements. TNR and DV take this opportunity to congratulate Prof. Sylvio Canuto on his 75th birthday. ND thanks the "Fonds de la Recherche Scientifique – FNRS" (F.R.S.–FNRS) and the Walloon Region for his FRIA grant. DV acknowledges funding by the F.R.S.–FNRS under Grant no. T.0226.24 (OMLED) for his postoctoral position. PB thanks the ECOBAT project (EOS no. 40007515) for his postoctoral position. TNR is a postdoctoral researcher of the F.R.S.–FNRS. Calculations were performed on the computers of the Consortium des Équipements de Calcul Intensif (CÉCI, http://www.ceci-hpc.be) and particularly those of the Technological Platform of High-Performance Computing (PTCI) of UNamur, for which the authors gratefully acknowledge the financial support of the FNRS-FRFC, of the Walloon Region, and of the University of Namur (Conventions no. U.G006.15, U.G018.19, U.G011.22, RW/GEQ2016, RW2210148, and RW2110213). The present research also benefited from computational resources made available on Lucia, the Tier-1 supercomputer of the Walloon Region, infrastructure funded by the Walloon Region under the grant agreement no. RW1910247.

Declarations

- **Funding**

  This research was supported by "Fonds de la Recherche Scientifique – FNRS" (F.R.S.–FNRS), the Walloon Region, and University of Namur. Grant numbers are listed in the Acknowledgements Section.

- **Conflict of interest**

  The authors declare no competing financial interest.

- **Data availability**

  In addition to the supplementary files, data can be obtained by contacting the corresponding authors.

- **Author contribution**

N. Deveaux: Data Curation, Formal Analysis, Investigation, Methodology, Software, Visualization, Writing – Original Draft, Writing – Review & Editing. **D. Valverde:** Data Curation, Formal Analysis, Investigation, Methodology, Visualization, Writing – Original Draft, Writing – Review & Editing. **P. Beaujean:** Formal Analysis, Investigation, Methodology, Software, Validation, Writing – Original Draft, Writing – Review & Editing. **B. Champagne:** Funding Acquisition, Project Administration, Resources, Supervision, Validation, Writing – Review & Editing. **T. N. Ramos:** Conceptualization, Data Curation, Formal Analysis, Investigation, Methodology, Resources, Software, Supervision, Validation, Visualization, Writing – Original Draft, Writing – Review & Editing.

References

[1] W.E. Proebster (ed.), *Digital Memory and Storage*, 1st edn. (Springer Vieweg, Braunschweig, Germany, 1978). https://doi.org/10.1007/978-3-322-83629-8

[2] B.L. Feringa, W.R. Browne (eds.), *Molecular Switches*, 2nd edn. (Wiley-VCH, Weinheim, Germany, 2011). https://doi.org/10.1002/9783527634408

[3] A.P. de Silva, *Molecular Logic-Based Computation*, 1st edn. (RSC Publishing, Cambridge, UK, 2013). https://doi.org/10.1039/9781849733021

[4] J. Andréasson, U. Pischel, Molecules with a sense of logic: A progress report. Chem. Soc. Rev. **44**, 1053–1069 (2015). https://doi.org/10.1039/c4cs00342j

[5] T. Kudernac, N. Katsonis, W.R. Browne, B.L. Feringa, Nano-electronic switches: Light-induced switching of the conductance of molecular systems. J. Mater. Chem. **19**, 7168–7177 (2009). https://doi.org/10.1039/b902009h

[6] X. Huang, T. Li, Recent progress in the development of molecular-scale electronics based on photoswitchable molecules. J. Mater. Chem. C **8**, 821–848 (2020). https:

//doi.org/10.1039/c9tc06054e

[7] M. Irie, T. Fukaminato, T. Sasaki, N. Tamai, T. Kawai, A digital fluorescent molecular photoswitch. Nature **420**, 759–760 (2002). https://doi.org/10.1038/420759a

[8] A. Mishra, A. Betal, N. Pal, R. Kumar, P. Lama, S. Sahu, R.K. Metre, Molecular memory switching device based on a tetranuclear organotin sulfide cage $[RS_n^{IV})_4(\mu - S)_6] \bullet 2CHCl_3 \bullet 4H_2O$ (R = 2-(Phenylazo)phenyl): synthesis, structure, DFT studies, and memristive behavior. ACS Appl. Electron. Mater. **2**, 220–229 (2020). https://doi.org/10.1021/acsaelm.9b00703

[9] M. Irie, T. Fukaminato, K. Matsuda, S. Kobatake, Photochromism of diarylethene molecules and crystals: Memories, switches, and actuators. Chem. Rev. **114**, 12174–12277 (2014). https://doi.org/10.1021/cr500249p

[10] T. Fukaminato, T. Sasaki, T. Kawai, N. Tamai, M. Irie, Digital photoswitching of fluorescence based on the photochromism of diarylethene derivatives at a single-molecule level. J. Am. Chem. Soc. **126**, 14843–14849 (2004). https://doi.org/10.1021/ja047169n

[11] L. Gobbi, P. Seiler, F. Diederich, V. Gramlich, C. Boudon, J.P. Gisselbrecht, M. Gross, Photoswitchable tetraethynylethene-dihydroazulene chromophores. Helv. Chim. Acta **84**, 743–777 (2001). https://doi.org/10.1002/1522-2675(20010418)84:4⟨743::AID-HLCA743⟩3.0.CO;2-1

[12] G. Szalöki, G. Sevez, J. Berthet, J.L. Pozzo, S. Delbaere, A simple molecule-based octastatesswitch. J. Am. Chem. Soc. **136**, 13510–13513 (2014). https://doi.org/10.1021/ja506320j

[13] Y. Aidibi, P. Beaujean, J. Quertinmont, J. Stiennon, M. Hodée, P. Leriche, J. Berthet, S. Delbaere, B. Champagne, L. Sanguinet, A molecular loaded dice: When the π conjugation breaks the statistical addressability of an octastate multimodal molecular switch. Dyes Pigm. **202**, 110270 (2022). https://doi.org/10.1016/J.DYEPIG.2022.110270

[14] M. Andreev, S. Seo, K.S. Jung, J.H. Park, Looking beyond 0 and 1: Principles and technology of multi-valued logic devices. Adv. Mater. **34**, 2108830 (2022). https://doi.org/10.1002/adma.202108830

[15] K. Szaciłowski, Digital information processing in molecular systems. Chem. Rev. **108**, 3481–3548 (2008). https://doi.org/10.1021/cr068403q

[16] M.M. Lerch, M.J. Hansen, W.A. Velema, W. Szymanski, B.L. Feringa, Orthogonal photoswitching in a multifunctional molecular system. Nat. Commun. **7**, 12054 (2016). https://doi.org/10.1038/ncomms12054

[17] M. Dowds, S.G. Stenspil, J.H. de Souza, B.W. Laursen, M. Cacciarini, M.B. Nielsen, Orthogonal- and path-dependent photo/acidoswitching in an eight-state dihydroazulene-spiropyran dyad. ChemPhotoChem **6**, e202200152 (2022). https://doi.org/10.1002/cptc.202200152

[18] S. Kawata, Y. Kawata, Three-dimensional optical data storage using photochromic materials. Chem. Rev. **100**, 1777–1788 (2000). https://doi.org/10.1021/cr980073p

[19] E. Walker, P.M. Rentzepis, Two-photon technology a new dimension. Nat. Photon. **2**, 406–408 (2008). https://doi.org/10.1038/nphoton.2008.121

[20] M. Zhao, J. Wen, Q. Hu, X. Wei, Y.W. Zhong, H. Ruan, M. Gu, A 3D nanoscale optical disk memory with petabit capacity. Nature **626**, 772–778 (2024). https:

//doi.org/10.1038/s41586-023-06980-y

[21] M.S. Kim, T. Sakata, T. Kawai, M. Irie, Amorphous photochromic films for near-field optical recording. Jpn. J. Appl. Phys. **42**, 3676–3681 (2003). https://doi.org/10.1143/jjap.42.3676

[22] R.W. Boyd, *Nonlinear Optics*, 4th edn. (Acadamic Press Elsevier, London, UK, 2020). https://doi.org/10.1016/C2015-0-05510-1

[23] M. Göppert-Mayer, Über elementarakte mit zwei quantensprüngen. Ann. Phys. (Leipzig) **401**, 273 (1931). https://doi.org/10.1002/andp.19314010303

[24] M. Göppert-Mayer, Elementary processes with two quantum transitions. Ann. Phys. **18**, 466–479 (2009). https://doi.org/10.1002/andp.200910358

[25] W. Kaiser, C.G.B. Garrett, Two-photon excitation in CaF_2: Eu^{2+}. Phys. Rev. Lett. **7**, 229–231 (1961). https://doi.org/10.1103/PhysRevLett.7.229

[26] M. Pawlicki, H.A. Collins, R.G. Denning, H.L. Anderson, Two-photon absorption and the design of two-photon dyes. Angew. Chem. Int. Ed. **48**, 3244–3266 (2009). https://doi.org/10.1002/anie.200805257

[27] L. Xu, W. Lin, B. Huang, J. Zhang, X. Long, W. Zhang, Q. Zhang, The design strategies and applications for organic multi-branched two-photon absorption chromophores with novel cores and branches: A recent review. J. Mater. Chem. C. **9**, 1520–1536 (2021). https://doi.org/10.1039/d0tc05910b

[28] M. Bravo-Romero, Óscar Guzmán-Méndez, M.M. Reza, J. Peon, Mechanism for the indirect photo-transformation of molecular switches using a pyrrolo–pyrrole two-photon absorbing antenna. ChemPhotoChem **9**, e202400229 (2025). https://doi.org/10.1002/cptc.202400229

[29] T. Verbiest, K. Clays, V. Rodriguez, *Second-Order Nonlinear Optical Characterization Techniques An Introduction* (CRC Press, New York, USA, 2009). https://doi.org/10.1201/9781420070736

[30] B.J. Coe, Molecular materials possessing switchable quadratic nonlinear optical properties. Chem. Eur. J. **5**, 2464–2471 (1999). https://doi.org/10.1002/(SICI)1521-3765(19990903)5:9⟨2464::AID-CHEM2464⟩3.0.CO;2-L

[31] J.A. Delaire, K. Nakatani, Linear and nonlinear optical properties of photochromic molecules and materials. Chem. Rev. **100**, 1817–1845 (2000). https://doi.org/10.1021/cr980078m

[32] F. Castet, V. Rodriguez, J.L. Pozzo, L. Ducasse, A. Plaquet, B. Champagne, Design and Characterization of Molecular Nonlinear Optical Switches. Accounts of Chemical Research **46**, 2656–2665 (2013). https://doi.org/10.1021/ar4000955

[33] M. Abedi, M. Pápai, K.V. Mikkelsen, N.E. Henriksen, K.B. Møller, Mechanism of photoinduced dihydroazulene ring-opening reaction. J. Phys. Chem. Lett. **10**, 3944–3949 (2019). https://doi.org/10.1021/acs.jpclett.9b01522

[34] I. Bayach, Y.S. Al-Faiyz, M.A. Alkhalifah, N. Almutlaq, K. Ayub, N.S. Sheikh, Phototunable absorption and nonlinear optical properties of thermally stable dihydroazulene-vinylheptafulvene photochrome pair. ACS Omega **7**, 35863–35874 (2022). https://doi.org/10.1021/acsomega.2c04231

[35] S. Shostak, W. Park, J. Oh, J. Kim, S. Lee, H. Nam, M. Filatov, D. Kim, C.H. Choi, Ultrafast excited state aromatization in dihydroazulene. J. Am. Chem. Soc. **145**, 1638–1648 (2023). https://doi.org/10.1021/jacs.2c09800

[36] L. Kortekaas, W.R. Browne, The evolution of spiropyran: Fundamentals and progress of an extraordinarily versatile photochrome. Chem. Soc. Rev. **48**,

3406–3424 (2019). https://doi.org/10.1039/c9cs00203k

[37] N. Deveaux, T.N. Ramos, P. Beaujean, F. Castet, B. Champagne, Quantum chemical study of a dihydroazulene-spiropyran multi-state multi-functional molecular switch. ChemPhotoChem **8**, e202400063 (2024). https://doi.org/10.1002/cptc.202400063

[38] W.R. Browne, B.L. Feringa, Light switching of molecules on surfaces. Annu. Rev. Phys. Chem. **60**, 407–428 (2009). https://doi.org/10.1146/annurev.physchem.040808.090423

[39] S.Z. Hassan, J. Kwon, J. Lee, H.R. Sim, S. An, S. Lee, D.S. Chung, Photophore-anchored molecular switch for high-performance nonvolatile organic memory transistor. Adv. Sci. **11**, 2401482 (2024). https://doi.org/10.1002/advs.202401482

[40] A.V. Kulinich, A.A. Ishchenko, Merocyanines: Electronic structure and spectroscopy in solutions, solid state, and gas phase. Chem. Rev. **124**, 12086–12144 (2024). https://doi.org/10.1021/acs.chemrev.4c00317

[41] D.A. Parthenopoulos, P.M. Rentzepis, Three-dimensional optical storage memory. Science **245**, 843–845 (1989). https://doi.org/10.1126/science.245.4920.843

[42] J. Zhang, H. Shen, X. Liu, X. Yang, S.L. Broman, H. Wang, Q. Li, J.W. Lam, H. Zhang, M. Cacciarini, M.B. Nielsen, B.Z. Tang, A dihydroazulene-based photofluorochromic AIE system for rewritable 4D information encryption. Angew. Chem. Int. Ed. **61**, e202208460 (2022). https://doi.org/10.1002/anie.202208460

[43] J.D. Chai, M. Head-Gordon, Long-range corrected hybrid density functionals with damped atom-atom dispersion corrections. Phys. Chem. Chem. Phys. **10**, 6615–6620 (2008). https://doi.org/10.1039/b810189b

[44] M.T.P. Beerepoot, D.H. Friese, N.H. List, J. Kongsted, K. Ruud, Benchmarking two-photon absorption cross sections: Performance of CC2 and CAM-B3LYP. Phys. Chem. Chem. Phys. **17**, 19306–19314 (2015). https://doi.org/10.1039/C5CP03241E

[45] M. Chołuj, M.M. Alam, M.T.P. Beerepoot, S.P. Sitkiewicz, E. Matito, K. Ruud, R. Zaleśny, Choosing bad versus worse: Predictions of two-photon-absorption strengths based on popular density functional approximations. J. Chem. Theory Comput. **18**, 1046–1060 (2022). https://doi.org/10.1021/acs.jctc.1c01056

[46] T. Yanai, D.P. Tew, N.C. Handy, A new hybrid exchange-correlation functional using the coulomb-attenuating method (CAM-B3LYP). Chem. Phys. Lett. **393**, 51–57 (2004). https://doi.org/10.1016/j.cplett.2004.06.011

[47] Dalton, a molecular electronic structure program, release Dalton2020.1 (2022). URL http://daltonprogram.org

[48] N.M. Thellamurege, H. Li, Note: FixSol solvation model and FIXPVA2 tessellation scheme. J. Chem. Phys. **137**, 246101 (2012). https://doi.org/10.1063/1.4773280

[49] J.M.H. Olsen, N.H. List, C. Steinmann, A.H. Steindal, M.S. Nørby, P. Reinholdt. Pelib: The polarizable embedding library (2021). https://doi.org/10.5281/zenodo.3967017

[50] P.R. Monson, W.M. McClain, Polarization dependence of the two-photon absorption of tumbling molecules with application to liquid 1-chloronaphthalene and benzene. J. Chem. Phys. **53**, 29–37 (1970). https://doi.org/10.1063/1.1673778

[51] B.J. Orr, J.F. Ward, Perturbation theory of thennon-linear optical polarization of an isolated system. Mol. Phys. **20**, 513–526 (1971). https://doi.org/10.1080/

00268977100100481

[52] D.L. Silva, R.C. Barreto, E.G. Lacerda, K. Coutinho, S. Canuto, One- and two-photon absorption of fluorescein dianion in water: A study using S-QM/MM methodology and ZINDO method. Spectrochim. Acta - A: Mol. Biomol. Spectrosc. **119**, 63–75 (2014). https://doi.org/10.1016/j.saa.2013.04.035

[53] W.M. McClain, Excited state symmetry assignment through polarized two-photon absorption studies of fluids. J. Chem. Phys. **55**, 2789–2796 (1971). https://doi.org/10.1063/1.1676494

[54] M. Sheik-Bahae, A. Said, T.H. Wei, D. Hagan, E. Van Stryland, Sensitive measurement of optical nonlinearities using a single beam. IEEE J. Quantum Electron. **26**, 760–769 (1990). https://doi.org/10.1109/3.53394

[55] M. Albota, D. Beljonne, J.L. Brédas, J.E. Ehrlich, J.Y. Fu, A.A. Heikal, S.E. Hess, T. Kogej, M.D. Levin, S.R. Marder, D. McCord-Maughon, J.W. Perry, H. Röckel, M. Rumi, G. Subramaniam, W.W. Webb, X.L. Wu, C. Xu, Design of organic molecules with large two-photon absorption cross sections. Science **281**, 1653–1656 (1998)

[56] T. Kogej, D. Beljonne, F. Meyers, J. Perry, S. Marder, J. Brédas, Mechanisms for enhancement of two-photon absorption in donor–acceptor conjugated chromophores. Chem. Phys. Lett. **298**, 1–6 (1998). https://doi.org/10.1016/S0009-2614(98)01196-8

[57] X. Zhou, A.M. Ren, J.K. Feng, X.J. Liu, Y.D. Zhang, The one-photon and two-photon absorption properties for porphyrin-derived monomers and dimers. ChemPhysChem **4**, 991–997 (2003). https://doi.org/10.1002/cphc.200300767

[58] X.J. Liu, J.K. Feng, A.M. Ren, X. Zhou, Theoretical studies of the spectra and two-photon absorption cross sections for porphyrin and carbaporphyrins. Chem. Phys. Lett. **373**, 197–206 (2003). https://doi.org/10.1016/S0009-2614(03)00577-3

[59] T.N. Ramos, L.R. Franco, D.L. Silva, S. Canuto, Calculation of the one- and two-photon absorption spectra of water-soluble stilbene derivatives using a multiscale QM/MM approach. J. Chem. Phys. **159**, 024309 (2023). https://doi.org/10.1063/5.0152308

[60] P. Cronstrand, Y. Luo, H. Ågren, Generalized few-state models for two-photon absorption of conjugated molecules. Chem. Phys. Lett. **352**, 262–269 (2002). https://doi.org/10.1016/S0009-2614(01)01454-3

[61] K. Ohta, S. Yamada, K. Kamada, A.D. Slepkov, F.A. Hegmann, R.R. Tykwinski, L.D. Shirtcliff, M.M. Haley, P. Sałek, F. Gel'mukhanov, H. Ågren, Two-photon absorption properties of two-dimensional π-conjugated chromophores: Combined experimental and theoretical study. J. Phys. Chem. A **115**, 105–117 (2011). https://doi.org/10.1021/jp107044w

[62] K. Kamada, T. Namikawa, S. Senatore, C. Matthews, P.F. Lenne, O. Maury, C. Andraud, M. Ponce-Vargas, B. Le Guennic, D. Jacquemin, P. Agbo, D.D. An, S.S. Gauny, X. Liu, R.J. Abergel, F. Fages, A. D'Aléo, Boron difluoride curcuminoid fluorophores with enhanced two-photon excited fluorescence emission and versatile living-cell imaging properties. Chem. - Eur. J. **22**, 5219–5232 (2016). https://doi.org/10.1002/chem.201504903

[63] L.M. Abegão, P. Baldeck, K. Kamada, Two-photon absorption spectral properties of three-branched carbazole dye for polymerization initiator: An experimental and theoretical study. Opt. Mater. **148** (2024). https://doi.org/10.1016/j.optmat.

2024.114908

[64] J. Olsen, P. Jørgensen, Linear and nonlinear response functions for an exact state and for an MCSCF state. J. Chem. Phys. **82**, 3235–3264 (1985). https://doi.org/10.1063/1.448223

[65] C. Hättig, O. Christiansen, P. Jørgensen, Multiphoton transition moments and absorption cross sections in coupled cluster response theory employing variational transition moment functionals. J. Chem. Phys. **108**, 8331–8354 (1998). https://doi.org/10.1063/1.476261

[66] P. Sałek, O. Vahtras, J. Guo, Y. Luo, T. Helgaker, H. Ågren, Calculations of two-photon absorption cross sections by means of density-functional theory. Chem. Phys. Lett. **374**, 446–452 (2003). https://doi.org/10.1016/S0009-2614(03)00681-X

[67] I.H. Nayyar, A.E. Masunov, S. Tretiak, Comparison of TD-DFT Methods for the Calculation of Two-Photon Absorption Spectra of Oligophenylvinylenes. J. Phys. Chem. C **117**, 18170–18189 (2013). https://doi.org/10.1021/jp403981d

[68] M. de Wergifosse, C.G. Elles, A.I. Krylov, Two-photon absorption spectroscopy of stilbene and phenanthrene: Excited-state analysis and comparison with ethylene and toluene. J. Chem. Phys. **146**, 174102 (2017). https://doi.org/10.1063/1.4982045

[69] M. Rossano-Tapia, J.M.H. Olsen, A. Brown, Two-photon absorption cross-sections in fluorescent proteins containing non-canonical chromophores using polarizable QM/MM. Front. Mol. Biosci **7**, 111 (2020). https://doi.org/10.3389/fmolb.2020.00111

[70] M. de Wergifosse, S. Grimme, Perspective on simplified quantum chemistry methods for excited states and response properties. J. Phys. Chem. A **125**, 3841–3851 (2021). https://doi.org/10.1021/acs.jpca.1c02362

[71] K.D. Nanda, S. Gulania, A.I. Krylov, Theory, implementation, and disappointing results for two-photon absorption cross sections within the doubly electron-attached equation-of-motion coupled-cluster framework. J. Chem. Phys. **158**, 054102 (2023). https://doi.org/10.1063/5.0135052

[72] M. de Wergifosse, S. Grimme, The eXact integral simplified time-dependent density functional theory (XsTD-DFT). J. Chem. Phys. **160** (2024). https://doi.org/10.1063/5.0206380

[73] S. Löffelsender, P. Beaujean, M. de Wergifosse, Simplified quantum chemistry methods to evaluate non-linear optical properties of large systems. WIREs Comput. Mol. Sci. **14**, e1695 (2024). https://doi.org/https://doi.org/10.1002/wcms.1695

[74] S.M. Parker, S. Roy, F. Furche, Unphysical divergences in response theory. J. Chem. Phys. **145**, 134105 (2016). https://doi.org/10.1063/1.4963749

[75] T. Lu, F. Chen, Multiwfn: A multifunctional wavefunction analyzer. J. Comput. Chem. **33**, 580–592 (2012). https://doi.org/10.1002/jcc.22885

[76] T. Lu, F. Chen, A comprehensive electron wavefunction analysis toolbox for chemists, Multiwfn. J. Chem. Phys. **161**, 082503 (2024). https://doi.org/10.1063/5.0216272

[77] J.B. Foresman, M. Head-Gordon, J.A. Pople, M.J. Frisch, Toward a systematic molecular orbital theory for excited states. J. Phys. Chem. **96**, 135–149 (1992). https://doi.org/10.1021/j100180a030

[78] C.W. Dirk, M.G. Kuzyk, Missing-state analysis: A method for determining the origin of molecular nonlinear optical properties. Phys. Rev. A **39**, 1219–1226 (1989). https://doi.org/10.1103/PhysRevA.39.1219

[79] F. Plasser, Theodore: A toolbox for a detailed and automated analysis of electronic excited state computations. J. Chem. Phys. **152**(8), 084108 (2020). https://doi.org/10.1063/1.5143076

[80] N.M. O'boyle, A.L. Tenderholt, K.M. Langner, cclib: A library for package-independent computational chemistry algorithms. J. Comput. Chem. **29**(5), 839–845 (2008). https://doi.org/https://doi.org/10.1002/jcc.20823

[81] K. Zhao, P.W. Liu, C.K. Wang, Y. Luo, Effects of structural fluctuations on two-photon absorption activity of interacting dipolar chromophores. J. Phys. Chem. B **114**(33), 10814–10820 (2010). https://doi.org/10.1021/jp103791s

[82] D.L. Silva, N.A. Murugan, J. Kongsted, Z. Rinkevicius, S. Canuto, H. Ågren, The Role of Molecular Conformation and Polarizable Embedding for One- and Two-Photon Absorption of Disperse Orange 3 in Solution. J. Phys. Chem. B **116**(28), 8169–8181 (2012). https://doi.org/10.1021/jp3032034

[83] Y. Şimşek, A. Brown, Two-photon absorption properties of gold fluorescent protein: A combined molecular dynamics and quantum chemistry study. J. Phys. Chem. B **122**(22), 5738–5748 (2018). https://doi.org/10.1021/acs.jpcb.8b00885

[84] T.N. Ramos, D.L. Silva, B.J. Cabral, S. Canuto, On the spectral line width broadening for simulation of the two-photon absorption cross-section of para-nitroaniline in liquid environment. J. Mol. Liq. **301**, 112405 (2020). https://doi.org/10.1016/j.molliq.2019.112405

[85] F. Castet, C. Tonnelé, L. Muccioli, B. Champagne, Predicting the second-order nonlinear optical responses of organic materials: The role of dynamics. Accounts of Chemical Research **55**, 3716–3726 (2022). https://doi.org/10.1021/acs.accounts.2c00616

[86] H. Ågren, I. Harczuk, O. Vahtras, Decomposition of molecular properties. Phys. Chem. Chem. Phys. **21**(5), 2251–2270 (2019). https://doi.org/10.1039/C8CP04340J

[87] M. de Wergifosse, S. Grimme, A Unified Strategy for the Chemically Intuitive Interpretation of Molecular Optical Response Properties. J. Chem. Theor. Comput. **16**(12), 7709–7720 (2020). https://doi.org/10.1021/acs.jctc.0c00990